

ROBIN PRE-TRAINING FOR THE DEEP RITZ METHOD

A PREPRINT

Luca Courte

University of Freiburg

luca.courte@mathematik.uni-freiburg.de

Marius Zeinhofer

University of Freiburg

marius.zeinhofer@mathematik.uni-freiburg.de

ABSTRACT

We compare different training strategies for the Deep Ritz Method for elliptic equations with Dirichlet boundary conditions and highlight the problems arising from the boundary values. We distinguish between an exact resolution of the boundary values by introducing a distance function and the approximation through a Robin Boundary Value problem. However, distance functions are difficult to obtain for complex domains. Therefore, it is more feasible to solve a Robin Boundary Value problem which approximates the solution to the Dirichlet Boundary Value problem, yet the naïve approach to this problem becomes unstable for large penalizations. A novel method to compensate this problem is proposed using a small penalization strength to pre-train the model before the main training on the target penalization strength is conducted. We present numerical and theoretical evidence that the proposed method is beneficial.

I INTRODUCTION

After exceptional success in machine learning, neural networks become increasingly popular in numerical analysis. Strategies to approximate solutions of partial differential equations (PDEs) based on neural networks can be traced back to Dissanayake and Phan-Thien (1994) and Lagaris et al. (1998). Their approaches are currently being revived and extended thanks to increased computational power and ease of implementation in frameworks like Tensorflow and PyTorch, see Sirignano and Spiliopoulos (2018); E and Yu (2018); Raissi and Karniadakis (2018); Li et al. (2020); Abadi et al. (2016); Paszke et al. (2019).

Presently, a common drawback of neural network based methods is their poor reliability – a failure to learn even a simple solution to a PDE is not uncommon, see Wang et al. (2020); van der Meer et al. (2020). In this note, we show that using the boundary penalty method known from the finite element literature, see for instance Babuška (1973), to approximately enforce Dirichlet boundary conditions in the Deep Ritz Method leads to such an unreliability. More precisely, large penalization parameters – albeit mandatory for an accurate solution – lead to highly fluctuating errors and sometimes even to a failure to approximate the solution at all. We present a pre-training strategy to alleviate this issue. The key idea is to pre-train the model using a small penalization parameter and subsequently to shift it by an optimal amount before conducting the training with the desired large penalization. This approach is supported by a theoretical motivation which shows that the difference between a (perfectly) pre-trained model and the true solution to the zero boundary value problem can be expanded in a orthonormal basis with the first basis function being constant. The shifting of the pre-trained model then corresponds to the elimination of the first Fourier coefficient.

Although our numerical results are conducted for the Poisson equation on model domains, the method is applicable to general domains and general elliptic equations and can easily be combined with more advanced optimization strategies as for example proposed by Cyr et al. (2020); Lee et al. (2021).

1.1 Organization

The paper is organized as follows. After clarifying notation in 1.2, we give a short introduction to the Deep Ritz Method and related error estimates in 1.3, then we give an overview of our main results and the numerical experiments in 1.4. We present the details and results of the numerical experiments in sections II, III and IV. Finally, we draw conclusions in section V.

1.2 Notation

On an open subset Ω of \mathbb{R}^d with boundary $\partial\Omega$, we denote the Sobolev spaces of square integrable functions with square integrable weak derivatives by $H^1(\Omega)$. The subspace of $H^1(\Omega)$ with zero boundary values in the trace sense is denoted by $H_0^1(\Omega)$. The reader is referred to Grisvard (2011) for the precise definitions and more information on Sobolev spaces. For multivariate, scalar valued functions, we use the symbol Δ for the Laplace operator and ∇ for the gradient. For a parameter θ in a parameter set $\Theta \subseteq \mathbb{R}^N$ we denote by u_θ the neural network function corresponding to θ .

1.3 The Deep Ritz Method

In this section we briefly recall the Deep Ritz Method and the corresponding error estimates for linear elliptic equations. In general, the Deep Ritz Method proposed by E and Yu (2018), transforms the variational formulation of a PDE – if available – into a finite dimensional optimization problem using neural network type functions as an ansatz class. For example, suppose we want to approximately solve

$$\begin{aligned} -\Delta u &= f & \text{in } \Omega \\ u &= 0 & \text{on } \partial\Omega, \end{aligned} \quad (1)$$

where Ω is an open and bounded set in \mathbb{R}^d . It is well known that for a function $u \in H_0^1(\Omega)$ and a right-hand side $f \in H_0^1(\Omega)^*$ it is equivalent to solve (1) and to be a minimizer of the following optimization problem

$$u \in \arg \min_{v \in H_0^1(\Omega)} \frac{1}{2} \int_{\Omega} |\nabla v|^2 dx - f(v). \quad (2)$$

Now, we want to minimize (2) over a class of neural network functions. However, it is unfeasible to enforce zero boundary values due to the unconstrained nature of neural networks. A solution is to use the boundary penalty method which allows to approximate (2) by an unconstrained problem. This approach was used by E and Yu (2018). More precisely, let $\lambda > 0$ be a fixed penalization parameter and denote by Θ a set of neural network parameters and consider the problem of finding a (quasi-)minimiser of the loss function

$$\mathcal{L}_\lambda : \Theta \rightarrow \mathbb{R}, \quad \mathcal{L}_\lambda(\theta) = \frac{1}{2} \int_{\Omega} |\nabla u_\theta|^2 dx - f(u_\theta) + \lambda \int_{\partial\Omega} u_\theta^2 ds \quad (3)$$

This is now an unconstrained optimisation problem that enforces zero boundary conditions approximately depending on the size of λ . To gain insight into the nature of this approach, we consider the energy, i.e., the loss function extended to all of $H^1(\Omega)$

$$E_\lambda : H^1(\Omega) \rightarrow \mathbb{R}, \quad E_\lambda(u) = \frac{1}{2} \int_{\Omega} |\nabla u|^2 dx - f(u) + \lambda \int_{\partial\Omega} u^2 ds$$

and its associated Euler Lagrange equation

$$\begin{aligned} -\Delta u &= f & \text{in } \Omega \\ \partial_n u + 2\lambda u &= 0 & \text{on } \partial\Omega. \end{aligned} \quad (4)$$

Thus, using (3) to approximate (1) means to use a Robin boundary value problem to approximate a Dirichlet condition. Müller and Zeinhofer (2021) have shown that under certain regularity conditions, the error introduced by this scheme can be bounded by

$$\|u_\theta - u_0\|_{H^1(\Omega)} \leq \|u_\theta - u_\lambda\|_{H^1(\Omega)} + \|u_\lambda - u_0\|_{H^1(\Omega)} \leq \sqrt{\frac{2\delta_\lambda}{\alpha_\lambda} + \frac{1}{\alpha_\lambda} \inf_{\tilde{\theta} \in \Theta} \|u_{\tilde{\theta}} - u_\lambda\|_\lambda^2} + C(\Omega) \cdot \|f\|_{L^2(\Omega)} \lambda^{-1}. \quad (5)$$

Here, u_0 denotes the solution to (1), u_λ is the solution to the Robin Boundary Value Problem (4) and u_θ is a realization of a neural network with parameters θ , e.g., produced through training. The remaining quantities are given by

$$\delta_\lambda = \mathcal{L}_\lambda(\theta) - \inf_{\tilde{\theta} \in \Theta} \mathcal{L}_\lambda(\tilde{\theta}), \quad \|\cdot\|_\lambda^2 = \|\nabla \cdot\|^2 + \lambda \|\cdot\|_{L^2(\partial\Omega)}^2, \quad \alpha_\lambda = \inf_{\|u\|_{H^1(\Omega)}=1} \|u\|_\lambda^2$$

and $C(\Omega)$ is a domain dependent constant. The estimate above indicates five potential sources of errors that guide our interpretation of the numerical experiments.

- (i) The error introduced by the fact that the Deep Ritz Method approximates a Robin Boundary Value Problem. This is encoded in the term

$$C(\Omega) \cdot \|f\|_{L^2(\Omega)} \lambda^{-1}.$$

- (ii) The optimization error made by the imperfect training. This is captured by the quantity

$$\frac{2\delta_\lambda}{\alpha_\lambda} = \frac{2}{\alpha_\lambda} \left(\mathcal{L}_\lambda(\theta) - \inf_{\tilde{\theta} \in \Theta} \mathcal{L}_\lambda(\tilde{\theta}) \right). \quad (6)$$

- (iii) The error due to the lack of expressiveness of the ansatz class

$$\inf_{\tilde{\theta} \in \Theta} \|u_{\tilde{\theta}} - u_\lambda\|_\lambda^2,$$

i.e., the distance of an ideal neural network from the Robin solution in the norm $\|\cdot\|_\lambda$.

- (iv) The error caused by the numerical approximation of the integrals in the loss function.

- (v) The error introduced by potentially large constants α_λ^{-1} and $C(\Omega)$.

Remark 1 (Sharpness of the Error Estimates). As we employ the triangle inequality in (5) it is unclear whether the estimate can be improved and might therefore be of limited use for discussing the errors observed in practice. However, for Dirichlet boundary conditions, we are interested in large values of λ and in that case the influence of the triangle inequality is marginal as u_λ approaches u_0 . Furthermore, the estimates of the two summands resulting from the triangle inequality's application are optimal. The first uses a Céa Lemma with the only estimate being a norm equivalence, compare to Proposition 3.1 in Müller and Zeinhofer (2021). The optimality of the second term follows by the observation that the solution to Dirichlet problem (1) on the disk differs by $\mathcal{O}(\lambda^{-1})$ from the solution of the Robin problem on the disk (4). We therefore deem the estimate (5) reliable to discuss the errors observed in practice.

1.4 Numerical Methods, Experiments & Main Results

We investigate and compare three approaches to deal with zero boundary values in the Deep Ritz Method. First, in section II as a naïve idea, we use the loss function \mathcal{L}_λ defined in (3) for a fixed $\lambda > 0$. It turns out that this method becomes increasingly unstable as λ increases. Furthermore, we find strong evidence that the most relevant error is due to the imperfect training, as listed in (6) above.

Second, as the direct usage of \mathcal{L}_λ is unreliable, we propose a novel two step scheme. In the first step we train the network for a small parameter λ_P , i.e., we use the loss function \mathcal{L}_{λ_P} . We refer to this step as the pre-training. Then, we choose our (large) target value λ_T , shift the function produced through the pre-training optimally with respect to \mathcal{L}_{λ_T} by a constant, and proceed with the training. See section III for a theoretical interpretation of this method and numerical results. We find that this approach increases accuracy and reduces the variance of the error over multiple runs.

Finally, we circumvent the penalty method completely by encoding zero boundary values directly into the model as originally proposed by Lagaris et al. (1998). The idea is to use a smooth function $d : \bar{\Omega} \rightarrow [0, \infty)$ that satisfies $d(x) = 0$ on $\partial\Omega$ and $d(x) > 0$ in Ω . We call d a smooth distance function. Then, the ansatz space for the minimization of (2) is chosen to be

$$\{u_\theta \cdot d \mid \theta \in \Theta\} \subset H_0^1(\Omega),$$

where Θ is a parameter set of a neural network architecture. Interestingly, we find that the choice of the smooth distance function has a significant influence on the accuracy of this approach, making an ideal choice difficult without a priori knowledge of the solution. Still, this approach performs best, with lowest error and variance. However, a smooth distance function is difficult or costly to obtain on complex domains. We refer the reader to Berg and Nyström (2018).

We compare these three methods for three different problems in two dimensions

- (i) on the disk, i.e., $\Omega = B_1(0)$ and $f \equiv 1$,
- (ii) on the annulus, i.e., $\Omega = B_2(0) \setminus B_1(0)$ and $f \equiv 1$,
- (iii) on the square, i.e., $\Omega = [0, 1]^2$ and $f(x_1, x_2) := 8\pi^2 \sin(2\pi x_1) \sin(2\pi x_2)$.

We chose these domains as exact solutions are analytically available and can be used to estimate the performance of the different optimization schemes. Indeed, we have

- (i) on the disk, the analytical solution is given by $u^D(x) := -\frac{1}{4}|x|^2 + \frac{1}{4}$ for $x \in B_1(0)$,
- (ii) on the annulus, the analytical solution is given by $u^A(x) := -\frac{1}{4}|x|^2 + \frac{3}{4\log(2)}\log(|x|) + \frac{1}{4}$ for $x \in B_2(0) \setminus B_1(0)$,
- (iii) on the square, the analytical solution is given by $u^S(x_1, x_2) := \sin(2\pi x_1)\sin(2\pi x_2)$ for $(x_1, x_2) \in [0, 1]^2$.

1.5 Discretization, Network Architecture & Optimization Routine

To the best of our knowledge, there is no consensus yet on which network architectures and optimization strategies are favorable for the approximation of PDE solutions. We use small networks with moderate depth to keep the computational cost manageable. Also in view of the discretization of the loss functional \mathcal{L}_λ in (3) this seems reasonable, compare to remark 2. Our precise choices that are global for all experiments are reported below.

- (i) We use fully connected feed forward networks with four hidden layers and input dimension two and output dimension one. All hidden layers have 14 neurons. We choose the hyperbolic tangent as our activation function.
- (ii) We initialize the weights using Glorot uniform initialization and the biases are initialized by zero.
- (iii) The numerical integration of the integrals for the training is done using fixed evaluation points. For a number $N \in \mathbb{N}$ we use points in the lattice $\frac{1}{N}\mathbb{Z}^2$ to approximate the integral of a function $f : \Omega \subset \mathbb{R}^2 \rightarrow \mathbb{R}$ via

$$\int_{\Omega} f dx = \frac{1}{N} \sum_{x_i \in \frac{1}{N}\mathbb{Z}^2 \cap \text{int}(\Omega)} f(x_i).$$

Integrals over the boundary of a domain are approximated using arclength parametrization with $N \cdot |\partial\Omega|$ many equi-spaced evaluation points. Here $|\partial\Omega|$ denotes the length of $\partial\Omega$. For the square and the annulus we use roughly 250,000 evaluation points, i.e., the lattice constants are $N = 500$ and $N = 160$ respectively. For the disk we use roughly 90000 evaluation points, i.e, $N = 160$. We refer the reader to remark 2 and Appendix C for a legitimisation of these choices.

- (iv) For the optimization process we use the Adam optimizer with 10000 iterations. Depending on the experiment we vary slightly with the learning rate. Details can be found in the corresponding sections.
- (v) The relative $L^2(\Omega)$ and $H^1(\Omega)$ errors are computed using 10^6 uniformly sampled evaluation points in Ω for every integral appearing in the respective norms.

Note that we do not employ a stochastic gradient descent. In our loss function, we do not introduce a batch size and in the approximation of the integrals in (3) we do not use random points. The only random effect is introduced through the networks weight initialization.

In the following, it will sometimes be important to distinguish between the continuous loss as stated in (3) and its numerical approximation which we call numerical loss function. It is given by applying the integral discretization described above to (3). More precisely, denoting by N_{int} and N_{bdr} the number of evaluation points (x_i) in the interior of Ω and (z_j) on its boundary $\partial\Omega$ we have

$$\mathcal{L}_\lambda^N : \Theta \rightarrow \mathbb{R}, \quad \theta \mapsto \frac{1}{N_{\text{int}}} \sum_{i=1}^{N_{\text{int}}} \left[\frac{1}{2} |\nabla u_\theta(x_i)|^2 - f(x_i)u_\theta(x_i) \right] + \frac{\lambda}{N_{\text{bdr}}} \sum_{j=1}^{N_{\text{bdr}}} u_\theta^2(z_j). \quad (7)$$

Remark 2 (A Warning). The numerical loss function is severely ill-posed on expressive sets of functions. For arbitrary λ consider

$$\mathcal{L}_\lambda^N : H^1(\Omega) \cap C^1(\overline{\Omega}) \rightarrow \mathbb{R} \quad \text{with} \quad u \mapsto \mathcal{L}_\lambda^N(u).$$

Then \mathcal{L}_λ^N is unbounded from below (and above) and does not admit a global minimizer. An arbitrary small value of \mathcal{L}_λ^N can be achieved by a function that is zero on $\partial\Omega$, has vanishing gradients on the evaluation points in the interior and takes large values on the interior evaluation points. However, for a fixed size

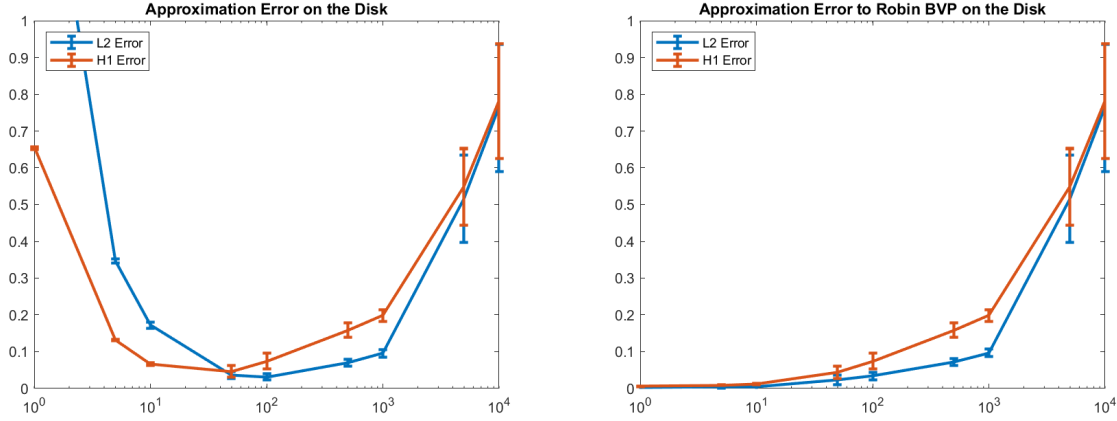


Figure 1: The expected relative error with its sample standard deviation for different values of λ on the disk with respect to the analytical solution of the Dirichlet BVP (on the left) and to the solution of the Robin BVP (on the right).

neural network this effect can be circumvented, provided enough evaluation points are used. This is another motivation to use small to medium size neural networks when working with the Deep Ritz Method in our setting.

II NAÏVE METHOD

We apply the Deep Ritz Method with boundary penalty to the equations listed in section 1.4. We use different but fixed penalization strengths and observe that large penalization values make the method unstable. We conclude that the decisive error contribution stems from the optimization.

Experiment Setup

For the three equations, we use the boundary penalization strengths $\lambda = 1, 5, 10, 50, 100, 500, 1000, 5000$ and 10000 and every experiment is conducted 25 times to capture the stochastic influence of the initialization. The optimization process is carried out with 10000 iterations of the Adam optimizer with learning rate 0.001. The remaining technical details such as network architecture and integral discretization are recorded in section 1.4 and do not differ across the different experiments in this note. We record the relative $L^2(\Omega)$ and $H^1(\Omega)$ errors. Furthermore, in the case of the disk and the annulus also the solutions u_D^λ and u_A^λ to the Robin problem (4) have an analytical form

$$u_D^\lambda(x) = -\frac{1}{4}(x_1^2 + x_2^2) + \frac{1}{4} + \frac{1}{4\lambda} \quad \text{and} \quad u_A^\lambda(x) = -\frac{|x|^2}{4} + C_1 \log(|x|) + C_2,$$

where

$$C_1 = \frac{1 + 2\lambda \left(\frac{3}{4} + \frac{1}{4\lambda}\right)}{\frac{1}{2} + 2\lambda \left(\log(2) + \frac{1}{2\lambda}\right)} \quad \text{and} \quad C_2 = \frac{C_1}{2\lambda} + \frac{1}{4} - \frac{1}{4\lambda}.$$

so we keep track of the relative $L^2(\Omega)$ and $H^1(\Omega)$ errors with respect to u_D^λ and u_A^λ as well.

Discussion

We report the relative errors in figure 1, figure 2, and figure 3 respectively. We observe a clear trade-off between too large and too small penalization parameters for all three equations. This is in accordance with the error estimates (5). We begin by investigating the experiment on the disk more closely. Specializing the error estimates to the case of the disk and estimating all unknown constants yields

$$\|u_\theta - u\|_{H^1(\Omega)} \leq \sqrt{\frac{8 + 10\lambda}{\lambda} \delta_\lambda + \frac{4 + 5\lambda}{\lambda} \inf_{\theta \in \Theta} \|u_\theta - u_\lambda\|_\lambda^2} + \frac{\pi}{4\lambda}.$$

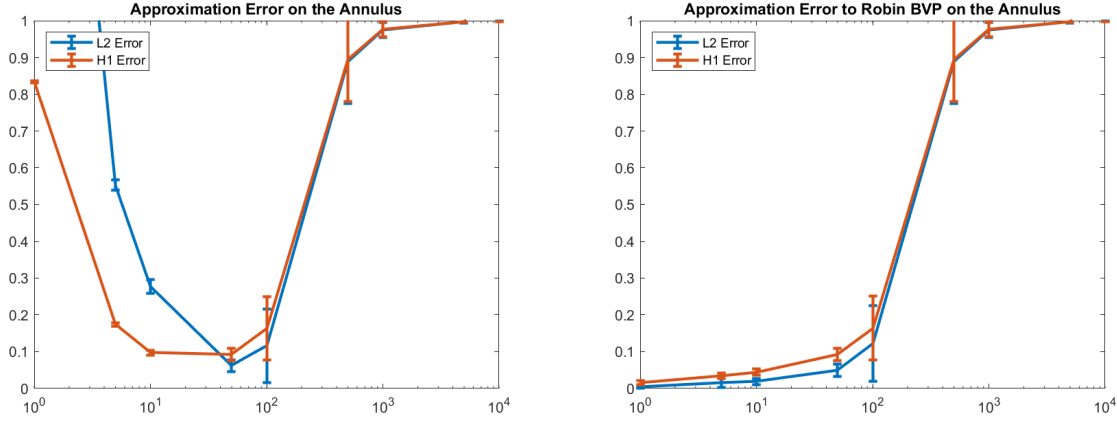


Figure 2: The expected relative error with its sample standard deviation for different values of λ on the annulus with respect to the analytical solution of the Dirichlet BVP (on the left) and to the solution of the Robin BVP (on the right).

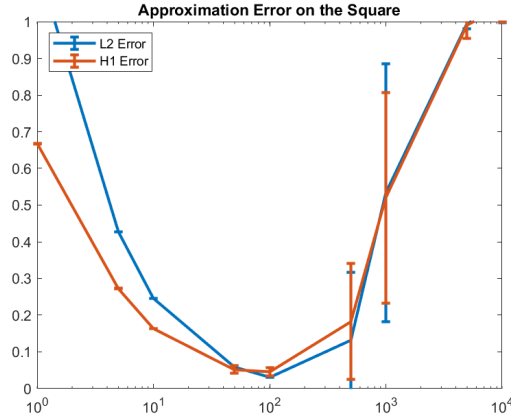


Figure 3: The expected relative error with its sample standard deviation for different values of λ on the square.

We refer the reader to Appendix A for the derivation of this estimate. The trade-off is due to the fact that the second term vanishes with $\lambda \rightarrow \infty$ but is large for small values of λ and in the first term both

$$\delta_\lambda = \mathcal{L}_\lambda(\theta) - \inf_{\tilde{\theta} \in \Theta} \mathcal{L}_\lambda(\tilde{\theta}) \quad \text{and} \quad \inf_{\tilde{\theta} \in \Theta} \|u_{\tilde{\theta}} - u_\lambda\|_\lambda^2 = \inf_{\tilde{\theta} \in \Theta} \left[\int_{\Omega} |\nabla(u_{\tilde{\theta}} - u_\lambda)|^2 dx + \lambda \int_{\partial\Omega} (u_{\tilde{\theta}} - u_\lambda)^2 ds \right]$$

can potentially be large for large values of λ . From the error plot in figure 1 (left) it is not immediately clear whether δ_λ or $\inf_{\tilde{\theta} \in \Theta} \|u_{\tilde{\theta}} - u_\lambda\|_\lambda^2$ introduces larger errors. However, a look at the solution to the Robin problem on the disk reveals that u_D^λ can be approximated – at least pointwise – in the same quality for every λ as different values of λ only correspond to different constant terms in u_D^λ which can be taken care of by the last bias of the approximating neural network. Still, the error to the Robin solution increases by a factor of over 100 with growing penalization strength and also the variance of the error over multiple runs increases drastically, see figure 1 (right).

A similar behavior is observed for the annulus, with high accuracy and low variance when measuring how well the Deep Ritz Method approximates the Robin solution for small penalization strengths. We refer to figure 2. In case of the square we do not have access to the Robin solution, yet an increasingly unstable training process is also clearly visible here, see figure 3. In particular, for all three equations a total failure to train, i.e., a relative error of around 100% frequently occurs in the large penalization regime. In this case the zero function is learned. Heuristically, we attribute the deteriorating accuracy to a growing number of

Table 1: Best relative errors with sample standard deviations

Domain	Best relative L^2 error	Best relative H^1 error
Disk	$(3.14 \pm 0.82) \cdot 10^{-2}$ achieved for $\lambda = 100$	$(4.61 \pm 1.61) \cdot 10^{-2}$ achieved for $\lambda = 50$
Annulus	$(6.19 \pm 1.55) \cdot 10^{-2}$ achieved for $\lambda = 50$	$(9.33 \pm 1.68) \cdot 10^{-2}$ achieved for $\lambda = 50$
Square	$(3.17 \pm 0.12) \cdot 10^{-2}$ achieved for $\lambda = 100$	$(4.62 \pm 1.14) \cdot 10^{-2}$ achieved for $\lambda = 100$

increasingly attractive, poor local minima in the loss landscape for large penalization strengths until for very large penalizations even the zero function can result from training. A large value of λ forces the gradient descent dynamics violently towards zero boundary conditions at the expense of other features of the PDEs solution, hence good minima become less attractive and difficult to find. For the experiments, the overall best performing λ are reported in table 1.

In our discussion so far, we did not take the numerical approximation of the integrals into account as the error estimates we used only hold for the continuous loss. As noted in remark 2 this is a potential source for errors. To exclude a relevant influence, we use a typical training session of one of the equations in section 1.4 and we monitor the loss for two different approximations of the integrals; one using the standard, medium fine grid and the other considerably finer. We conclude that the error introduced by the integral approximation can be neglected and refer to Appendix C for the details.

III REFINED METHOD

In the previous experiment, we have seen that the naïve approach using the boundary penalty method introduces large errors and unstable training dynamics, especially when compared to the essential boundary conditions of the Robin problem, i.e, the case when λ is small. To mitigate this effect, we propose to conduct a pre-training using a low penalization strength. The motivation behind this strategy is a similarity of the solution u_λ to the Robin problem (4) and the solution u_0 to the Dirichlet problem (1). We find that the proposed pre-training significantly reduces both the errors and the errors' variance.

3.1 Experiment Setup

We consider the equations listed in section 1.4. The following training strategy is used

- (i) We set a pre-training penalization strength, in our case $\lambda_P = 1$, and train the model using the loss function \mathcal{L}_{λ_P} for 4000 iterations with the Adam optimizer. Here the first 1000 iterations the learning rate is set to 0.01 and for the remaining 3000 iterations we use 0.001. Let us denote the the neural network realization that results from this training by u_{θ_P} .
- (ii) As target penalization strengths we use $\lambda_T = 1, 5, 10, 50, 100, 500, 1000, 5000, 10000$, and shift the network function u_{θ_P} adding a optimal constant t_{λ_T} namely

$$\tilde{u}_{\theta_P} = u_{\theta_P} + t_{\lambda_T} = u_{\theta_P} + \frac{1}{2\lambda_T|\partial\Omega|} \int_{\Omega} f(x) dx - \frac{1}{|\partial\Omega|} \int_{\partial\Omega} u_{\theta_P}(x) dx.$$

We denote the shifted function by \tilde{u}_{θ_P} . Finally we train \tilde{u}_{θ_P} for 6000 iterations with the Adam optimizer with learning rate 0.001 and the loss function \mathcal{L}_{λ_T} to conclude the training.

A theoretical motivation for this approach is given in section 3.3.

3.2 Discussion

Table 2: Best relative errors with sample standard deviations with pre-training

Domain	Best relative L^2 error	Best relative H^1 error
Disk	$(0.63 \pm 0.48) \cdot 10^{-2}$ achieved for $\lambda = 500$	$(1.17 \pm 0.21) \cdot 10^{-2}$ achieved for $\lambda = 500$
Annulus	$(1.81 \pm 0.80) \cdot 10^{-2}$ achieved for $\lambda = 500$	$(1.97 \pm 0.47) \cdot 10^{-2}$ achieved for $\lambda = 100$
Square	$(3.05 \pm 0.21) \cdot 10^{-2}$ achieved for $\lambda = 100$	$(4.54 \pm 0.48) \cdot 10^{-2}$ achieved for $\lambda = 100$

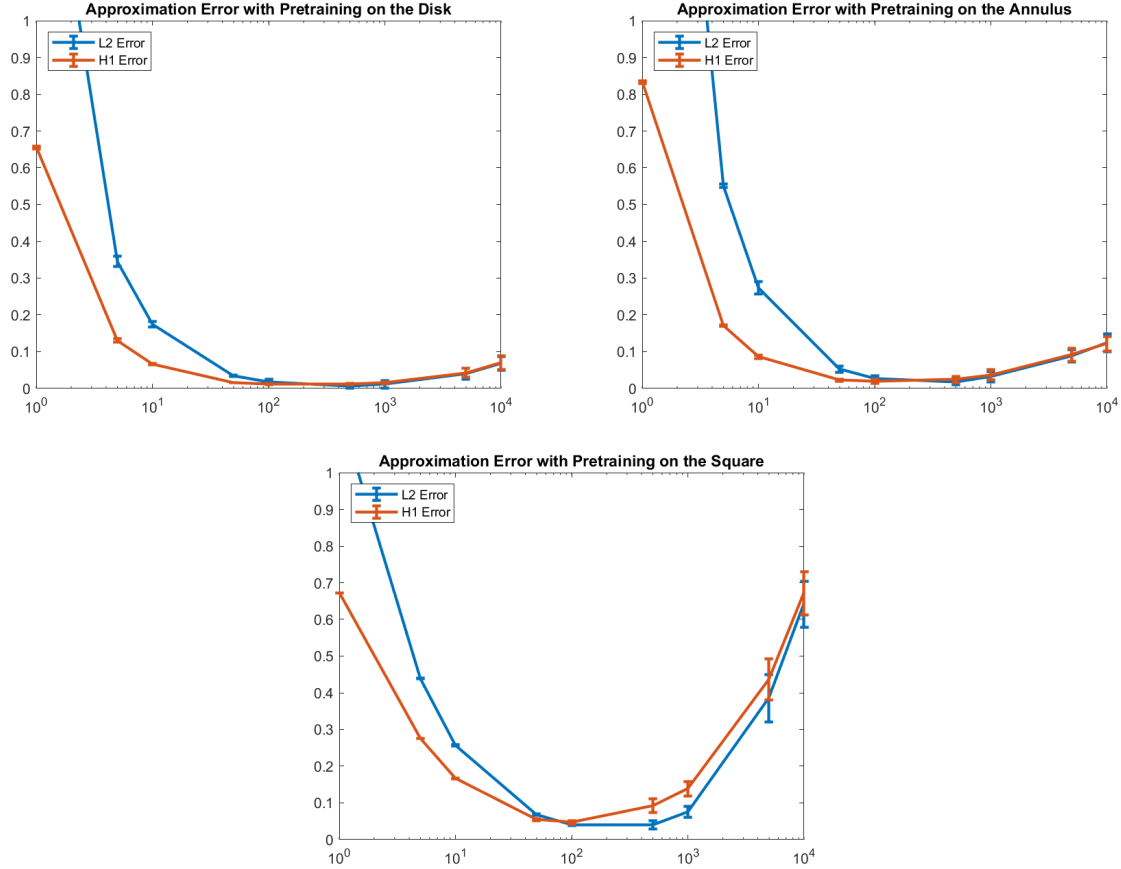


Figure 4: The expected relative error with its sample standard deviation for different values of λ with pre-training.

We report the relative $L^2(\Omega)$ and $H^1(\Omega)$ errors obtained through using the proposed pre-training strategy in figure 4 and the best results we obtained in table 2. We clearly see beneficial effects for both the accuracy and the variance of the errors for all three equations. In case of the disk, the relative error is almost reduced by a full magnitude. Also on the annulus, we see a drastic improvement of accuracy. For the square, the improvement in accuracy is smaller, however, the variance in the reported errors is decreased drastically as well. This is no surprise as the example of the square possesses an oscillating solution in the interior and we believe that the main error is due to this comparatively complicated solution. In the following, we list the advantages of our proposed pre-training strategy.

- (i) Improved accuracy and increased reliability as discussed above.
- (ii) Potential computational savings. Even though our method requires to pre-train the model we believe that the overall computational cost can be reduced. In fact, using larger learning rates is possible as the loss landscape is less rough for small values of λ . We have already exploited this in our experiment setup. Also in the main training, potentially larger learning rates can be used as the model is already in a reasonable state. We leave the fine-tuning of learning rate schedules for future research.
- (iii) Decreased sensitivity to the choice of penalization parameter. Particularly, the experiments on the disk and the annulus suggest that the accuracy of the method does not depend as strongly on the penalization strength as in the case without pre-training. This facilitates choosing a reasonable penalization strength.

3.3 Theoretical Motivation for Pre-Training

In this section we justify our pre-training and especially the shift by a constant value. Remember that the boundary penalty method with penalty parameter λ corresponds to a Robin boundary value problem as explained in (4). For the convenience of the reader we repeat the equation

$$\begin{aligned} -\Delta u &= f & \text{in } \Omega \\ \partial_n u + 2\lambda u &= 0 & \text{on } \partial\Omega, \end{aligned}$$

and we denote its solution by u_λ . Heuristically, letting $\lambda \rightarrow \infty$ we recover the Dirichlet problem

$$\begin{aligned} -\Delta u &= f & \text{in } \Omega \\ u &= 0 & \text{on } \partial\Omega, \end{aligned}$$

with solution u_0 . Our motivation for optimizing among constants stems from the fact that the difference $v_\lambda := u_0 - u_\lambda$ can be expanded in a suitable orthonormal basis $(e_j)_{j \in \mathbb{N}}$ – a Steklov eigenbasis – and is given by

$$v_\lambda = \sum_{j=0}^{\infty} c_j e_j, \quad (8)$$

where in fact the leading basis function is constant. Thus, our suggested shifting by a constant eliminates this leading term and brings the result of the pre-training closer to the desired solution of the Dirichlet problem. The details of the expansion (8) will be provided in the appendix. To determine the optimal constant by which a pre-trained model should be shifted, a simple analytical argument suffices.

Proposition 3. *Let $\lambda > 0$ and $L : \mathbb{R}^n \times \mathbb{R}^n \rightarrow \mathbb{R}$ a Lagrangian and $u_0 : \mathbb{R}^n \rightarrow \mathbb{R}$ an admissible function, then the energy*

$$E_\lambda[u] := \int_{\Omega} L(x, \nabla u(x)) \, dx - \int_{\Omega} f(x)u(x) \, dx + \lambda \int_{\partial\Omega} |u(x)|^2 \, dx$$

is minimized among all translations $u_t := u_0 + t$ for $t \in \mathbb{R}$ if

$$t = \tilde{t} := \frac{1}{2\lambda|\partial\Omega|} \int_{\Omega} f(x) \, dx - \frac{1}{|\partial\Omega|} \int_{\partial\Omega} u(x) \, dx.$$

Proof. The translation u_t for $t \in \mathbb{R}$ that minimizes the energy E_λ has to satisfy

$$\frac{d}{dt} E_\lambda[u + t] = 0.$$

Hence, it has to hold

$$0 = - \int_{\Omega} f(x)u(x) \, dx + 2\lambda \int_{\partial\Omega} u(x) + t \, dx$$

which, after rearranging, implies the stated equation for the translation $\tilde{t} \in \mathbb{R}$. Due to the structure of the energy this has to be a minimizer. □

Remark 4. The above motivation is not limited to the Laplace operator. In fact, also for the class of self-adjoint elliptic equations the Steklov theory holds and an analogue argument can be made. Note also, that the derivation of the optimal shifting applies to more general elliptic operators as well.

IV EXACT RESOLUTION OF BOUNDARY VALUES

We encode the zero boundary conditions directly into the network architecture using a smooth distance function to the boundary as described in section 1.4. For every domain we use two different distance functions and observe that the choice of this function has a considerable influence on the accuracy of the method. We conclude that this approach has the potential to be the most accurate but introduces a possibly hard to obtain and difficult to choose hyperparameter – the distance function.

4.1 Experiment Setup

We consider again the three equations introduced in section 1.4. For each domain we use two different smooth distance functions. One is based on trigonometric functions and the other is polynomial. Especially for the experiments on the disk and the annulus the trigonometric functions are chosen to prevent a too strong similarity with the solutions of the boundary value problems. More precisely we use

$$d_{\text{trig}}^D(r) = \cos\left(\frac{\pi r}{2}\right) \quad \text{and} \quad d_{\text{pol}}^D(r) = r^2 - 1$$

for the disk,

$$d_{\text{trig}}^S(x, y) = \sin(\pi x) \sin(\pi y) \quad \text{and} \quad d_{\text{pol}}^S(x, y) = x(x-1)y(y-1)$$

for the square and

$$d_{\text{trig}}^A(r) = \sin(\pi r) \quad \text{and} \quad d_{\text{pol}}^A(r) = -(r-1)(r-2)$$

for the annulus, with $r = \sqrt{x^2 + y^2}$. The optimization process is carried out using 10000 iterations of the Adam optimizer with learning rate 0.001 and every experiment (i.e., every domain-distance function pair) is repeated 25 times to capture the effect of the random initialization. The remaining hyperparameters are chosen as in the other experiments, see section 1.4 for an overview.

4.2 Discussion

We report the relative $L^2(\Omega)$ and relative $H^1(\Omega)$ errors in table 3. Comparing with the results of the previous experiments, see table 1 and table 2, we see that for both choices of distance functions this method is the most accurate for all three domains. However, the choice of the specific distance function has a drastic influence on the accuracy. In the case of the annulus the polynomial function performs by half a magnitude better and in the case of the disk by a factor of roughly three. We believe this phenomenon is due to the similarity of the polynomial distance function to the solutions of the PDEs. In the case of the disk, the solution is polynomial and in the case of the annulus, it is a sum of a polynomial and a logarithm, see section 1.4.

Finally, the conducted experiments with exact boundary conditions suggest that it is reasonable to use such a construction when available. However, the choice of the distance function has a significant influence on the accuracy of the method. Hence, without a priori knowledge of the solution making a good choice remains an open problem. Furthermore, on complex domains it is difficult and computationally expensive to produce such a distance function and can in general only be done approximately. We refer to Berg and Nyström (2018).

Table 3: Relative Errors for different choices of distance functions

Domain	L^2 error with d_{trig}	H^1 error with d_{trig}	L^2 error with d_{pol}	H^1 error with d_{pol}
Disk	$(0.37 \pm 0.58) \cdot 10^{-2}$	$(0.7 \pm 0.55) \cdot 10^{-2}$	$(0.14 \pm 0.17) \cdot 10^{-2}$	$(0.21 \pm 0.18) \cdot 10^{-2}$
Annulus	$(0.92 \pm 1.15) \cdot 10^{-2}$	$(1.67 \pm 0.97) \cdot 10^{-2}$	$(0.18 \pm 0.13) \cdot 10^{-2}$	$(0.29 \pm 0.11) \cdot 10^{-2}$
Square	$(1.09 \pm 1.1) \cdot 10^{-2}$	$(1.4 \pm 0.4) \cdot 10^{-2}$	$(0.64 \pm 0.04) \cdot 10^{-2}$	$(1.78 \pm 0.29) \cdot 10^{-2}$

V CONCLUSIONS

We discussed three different approaches to practically realize homogeneous Dirichlet boundary conditions in the Deep Ritz Method for elliptic equations. First, the naïve ansatz of using the boundary penalty method for a fixed penalization strength. Second, we proposed a novel strategy where the model is pre-trained using a small penalization parameter before conducting the main training for the target penalization. Finally, we enforced the boundary conditions directly into the ansatz functions by using a smooth distance function.

We found that the naïve approach suffers severely from the instability introduced by large penalization parameters which complicate the training process. This leads to imprecise approximation of the solution and a high variance of the errors. To alleviate this problem, the use of a smooth distance function seems beneficial, especially if one can encode intuition of the solution into the design of the distance function.

However, this is seldom possible for complicated domains. In this case, the proposed pre-training strategy can be used without extra computational or algorithmic cost. It is shown that this approach improves both accuracy and reduces the variance of the errors.

Future research directions are the fine-tuning of the proposed pre-training method, such as employing learning rate schedules and the overall reduction of computational cost. Furthermore, we propose to investigate how the method performs on more complex problems, especially paired with more elaborate training algorithms, for example the ones proposed in Cyr et al. (2020).

ACKNOWLEDGEMENT

LC gratefully acknowledges support from the Fonds National de la Recherche, Luxembourg (AFR Grant 13502370). MZ gratefully acknowledges support from BMBF within the e:Med program in the SyMBoD consortium (grant number 01ZX1910C). The authors thank Johannes Müller for valuable discussions and suggestions.

DECLARATION OF INTEREST

Declarations of interest: none.

REFERENCES

- Abadi, M., Barham, P., Chen, J., Chen, Z., Davis, A., Dean, J., Devin, M., Ghemawat, S., Irving, G., Isard, M., et al. (2016). Tensorflow: A system for large-scale machine learning. In *12th {USENIX} symposium on operating systems design and implementation ({OSDI} 16)*, pages 265–283.
- Auchmuty, G. (2005). Steklov eigenproblems and the representation of solutions of elliptic boundary value problems. *Numerical Functional Analysis and Optimization*, 25(3-4):321–348.
- Babuška, I. (1973). The finite element method with penalty. *Mathematics of computation*, 27(122):221–228.
- Berg, J. and Nyström, K. (2018). A unified deep artificial Neural Network Approach to Partial Differential Equations in complex Geometries. *Neurocomputing*, 317:28–41.
- Cyr, E. C., Gulian, M. A., Patel, R. G., Perego, M., and Trask, N. A. (2020). Robust Training and Initialization of Deep Neural Networks: An adaptive Basis Viewpoint. In *Mathematical and Scientific Machine Learning*, pages 512–536. PMLR.
- Dissanayake, M. and Phan-Thien, N. (1994). Neural-Network-based Approximations for solving Partial Differential Equations. *Communications in Numerical Methods in Engineering*, 10(3):195–201.
- E, W. and Yu, B. (2018). The Deep Ritz method: a Deep Learning-based numerical Algorithm for solving Variational Problems. *Communications in Mathematics and Statistics*, 6(1):1–12.
- Grisvard, P. (2011). *Elliptic Problems in nonsmooth Domains*. SIAM.
- Kovařík, H. (2014). On the lowest eigenvalue of laplace operators with mixed boundary conditions. *The Journal of Geometric Analysis*, 24(3):1509–1525.
- Lagaris, I. E., Likas, A., and Fotiadis, D. I. (1998). Artificial Neural Networks for solving Ordinary and Partial Differential Equations. *IEEE transactions on neural networks*, 9(5):987–1000.
- Lee, K., Trask, N. A., Patel, R. G., Gulian, M. A., and Cyr, E. C. (2021). Partition of unity networks: deep hp-approximation. *arXiv preprint arXiv:2101.11256*.
- Li, Z., Kovachki, N., Azizzadenesheli, K., Liu, B., Bhattacharya, K., Stuart, A., and Anandkumar, A. (2020). Fourier neural operator for parametric partial differential equations. *arXiv preprint arXiv:2010.08895*.
- Müller, J. and Zeinhofer, M. (2021). Error Estimates for the Variational Training of Neural Networks with Boundary Penalty. *arXiv preprint arXiv:2103.01007*.

Paszke, A., Gross, S., Massa, F., Lerer, A., Bradbury, J., Chanan, G., Killeen, T., Lin, Z., Gimelshein, N., Antiga, L., et al. (2019). Pytorch: An imperative style, high-performance deep learning library. *arXiv preprint arXiv:1912.01703*.

Raissi, M. and Karniadakis, G. E. (2018). Hidden physics models: Machine learning of nonlinear partial differential equations. *Journal of Computational Physics*, 357:125–141.

Sirignano, J. and Spiliopoulos, K. (2018). DGM: A Deep Learning Algorithm for solving Partial Differential Equations. *Journal of computational physics*, 375:1339–1364.

van der Meer, R., Oosterlee, C., and Borovykh, A. (2020). Optimally weighted Loss Functions for solving PDEs with Neural Networks. *arXiv preprint arXiv:2002.06269*.

Wang, S., Teng, Y., and Perdikaris, P. (2020). Understanding and mitigating gradient pathologies in physics-informed neural networks. *arXiv preprint arXiv:2001.04536*.

A DERIVATION OF ERROR ESTIMATES ON THE DISK

We provide the details for the specialized error estimates on the disk on which we base our discussion in section II.

Lemma 5. *Let $\Omega = B_1(0) \subset \mathbb{R}^2$ be the unit disk. Fix $\lambda > 0$ and let Θ denote a parameter set of some neural network architecture with $u_\theta \in H^1(\Omega)$ for all $\theta \in \Theta$. We denote by u_0 the solution to (1), by u_λ the solution to (4) and we let θ be arbitrary. Then it holds*

$$\|u_\theta - u_0\|_{H^1(\Omega)} \leq \sqrt{\frac{8 + 10\lambda}{\lambda} \delta_\lambda + \frac{4 + 5\lambda}{\lambda} \inf_{\theta \in \Theta} \|u_\theta - u_\lambda\|_\lambda^2} + \frac{\pi}{4\lambda}$$

where, using \mathcal{L}_λ as in (3), we have

$$\delta_\lambda = \mathcal{L}_\lambda(\theta) - \inf_{\theta \in \Theta} \mathcal{L}_\lambda(\tilde{\theta}) \quad \text{and} \quad \|\cdot\|_\lambda^2 = \|\nabla \cdot\|_{L^2(\Omega)}^2 + \lambda \|\cdot\|_{L^2(\partial\Omega)}^2$$

Proof. The error estimates derived by Müller and Zeinhofer (2021) yield

$$\|u_\theta - u_0\|_{H^1(\Omega)} \leq \sqrt{\frac{2\delta_\lambda}{\alpha_\lambda} + \frac{1}{\alpha_\lambda} \inf_{\theta \in \Theta} \|u_\theta - u_\lambda\|_\lambda^2} + \|u_\lambda - u_0\|_{H^1(\Omega)}.$$

Inspecting the solution formulas for u_0 and u_λ in section 1.4 reveals that $u_\lambda - u_0 \equiv \frac{1}{4\lambda}$, hence

$$\|u_\lambda - u_0\|_{H^1(\Omega)} = \frac{\pi}{4\lambda}.$$

It remains to estimate α_λ , the coercivity constant of the bilinear form

$$a_\lambda : H^1(\Omega) \times H^1(\Omega) \rightarrow \mathbb{R}, \quad a_\lambda(u, v) = \int_\Omega \nabla u \nabla v dx + \lambda \int_{\partial\Omega} uv ds.$$

In fact, α_λ may be estimated using the Friedrich's constant $C_{F,\lambda}$

$$\alpha_\lambda \geq (C_{F,\lambda} + 1)^{-1},$$

where $C_{F,\lambda}$ is the smallest constant satisfying

$$\int_\Omega u^2 dx \leq C_{F,\lambda} \left(\int_\Omega |\nabla u|^2 dx + \lambda \int_{\partial\Omega} u^2 ds \right) \quad \text{for all } u \in H^1(\Omega).$$

Furthermore, $C_{F,\lambda}$ can be connected to the first eigenvalue of the Robin Laplacian which we denote by μ_1^λ . More precisely it holds via the Rayleigh quotient characterization

$$\mu_1^\lambda = \min_{u \in H^1(\Omega) \setminus \{0\}} \frac{\int_\Omega |\nabla u|^2 dx + \lambda \int_{\partial\Omega} u^2 ds}{\int_\Omega u^2 dx} = C_{F,\lambda}^{-1}.$$

Finally, in the case of convex domains, two-sided estimates for μ_1^λ are known, see Kovařík (2014). In particular we get for the disk (as a general convex domain)

$$\mu_1^\lambda \geq \frac{\lambda}{4 + 4\lambda}$$

which concludes the proof. \square

B STEKLOV EIGENVALUE THEORY

We will now provide the details of the expansion (8) and repeat briefly the prerequisites from the Steklov eigenvalue theory. For the proofs of our basic results we refer to Müller and Zeinhofer (2021) and for a more advanced and comprehensive introduction to the Steklov Eigenvalue Theory the reader is referred to Auchmuty (2005). The basic definition in case of the Laplacian is the following.

Definition 6. Let $\Omega \subset \mathbb{R}^d$ be open and bounded. The Steklov eigenvalue problem for the Laplacian consists of finding $(\mu, w) \in \mathbb{R} \times H^1(\Omega) \setminus \{0\}$ such that

$$\int_{\Omega} \nabla w \nabla \varphi dx = \mu \int_{\partial\Omega} w \varphi ds \quad \text{for all } \varphi \in H^1(\Omega). \quad (9)$$

We call μ a *Steklov eigenvalue* and w a corresponding *Steklov eigenfunction*.

It is clear from the definition that constant functions are eigenfunctions to the eigenvalue zero. The main reason for considering Steklov eigenfunctions is that they provide an orthonormal basis for the weakly harmonic functions $\mathcal{H}(\Omega) = \{u \in H^1(\Omega) \mid -\Delta u = 0 \text{ in } H_0^1(\Omega)^*\}$.

Theorem 7 (Steklov spectral theorem). *Let Ω be a bounded Lipschitz domain. Then there exists a non decreasing sequence $(\mu_j)_{j \in \mathbb{N}} \subseteq [0, \infty)$ with $\mu_j \rightarrow \infty$ and $(e_j)_{j \in \mathbb{N}} \subseteq \mathcal{H}(\Omega)$ such that μ_j is a Steklov eigenvalue with eigenfunction e_j . Further, $(e_j)_{j \in \mathbb{N}}$ is a complete orthonormal system in $\mathcal{H}(\Omega)$ with respect to the inner product $a(u, v) = \int_{\Omega} \nabla u \nabla v dx + \int_{\partial\Omega} uv ds$ on $H^1(\Omega)$.*

This allows us to establish (8) rigorously.

Lemma 8. *Assume that $f \in H^1(\Omega)^*$ and suppose u_0 satisfies a homogeneous Dirichlet problem as in (1) and u_{λ} satisfies a homogeneous Robin problem as in (4), then $v_{\lambda} = u_0 - u_{\lambda}$ is a member of $\mathcal{H}(\Omega)$ and can be expanded in the form (8).*

Proof. This follows directly from Theorem 7. □

C INTEGRAL DISCRETIZATION

Here we discuss the influence of the approximation of the integrals in the loss function (3). As mentioned in remark 2 the discretized loss function is ill-posed on expressive sets of ansatz functions.

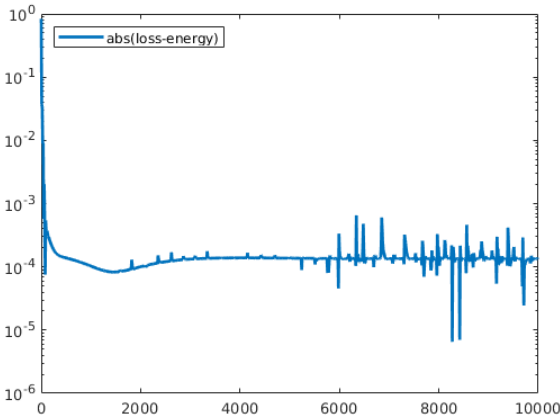


Figure 5: Evolution of the absolute value of the difference of the loss and the energy over the training process.

To investigate whether this ill-posedness leads to relevant errors we consider the experiments on the disk, the annulus and the square as described in section 1.4. For the disk, we conduct a training using roughly 90000 evaluation points in the interior and 1000 evaluation points on the boundary to approximate the integrals. More precisely, for the integral over $B_1(0)$ we use a $\varepsilon \cdot \mathbb{Z}^2$ grid with $\varepsilon = 1/160$. These were the values we employed in the other experiments throughout the article as well. Furthermore, we use a fixed penalization strength of $\lambda = 100$ and 10000 iterations of the Adam optimizer with learning rate 0.001. The remaining hyperparameters are chosen as reported in section 1.4. To monitor the influence of the discretization, at every tenth step of the optimization process we compute the value of the loss function in two ways. On the one hand using the 90000 evaluation points that are seen while training and on the other we use a million uniformly drawn evaluation points in the interior and 10000 on the boundary to capture a possible deviation of the two. We refer to the latter as the “energy” in contrast

the boundary to capture a possible deviation of the two. We refer to the latter as the “energy” in contrast

to the loss used for training. In figure 5, we present the evolution of the two quantities over the training process.

We observe that the loss and the energy differ by a value of magnitude 10^{-4} apart from occasional oscillations. We attribute these oscillations to a comparatively large learning rate as the loss function itself does exhibit oscillations as well¹. Especially, no consistent increase of the energy-loss difference is visible in the late training process, where overfitting would be expected. We therefore conclude that the numerical approximation of the integrals does not significantly contribute to the error of the Deep Ritz Method in our experiments.

For the annulus and the square, we conduct analogous experiments. For these domains, we use roughly 250000 evaluation points, i.e., we use a $\varepsilon \cdot \mathbb{Z}^2$ grid with $\varepsilon = 1/160$ for the annulus and $\varepsilon = 1/500$ for the square. In the case of the annulus, the absolute value of the difference of the energy and the loss is around 10^{-3} and in the case of the square it is as large as 10^{-1} . However, this large value for the square experiment can be explained by the fact that in the right-hand side of this equation the large factor $8\pi^2$ appears.

¹For brevity, no figure is provided.